Large Signal Stability Assessment of MPC-based Control for HVDC Electrical Grid

Tarcar, Rohan Kamat; Shetgaonkar, Ajay; Popov, Marjan; Lekić, Aleksandra

DOI
10.1109/ISGTEUROPE62998.2024.10863193

Publication date
2024

Document Version
Final published version

Published in
IEEE PES Innovative Smart Grid Technologies Europe, ISGT EUROPE 2024

Large Signal Stability Assessment of MPC-based Control for HVDC Electrical Grid

Rohan Kamat Tarcar, *Student Member, IEEE*, Ajay Shetgaonkar, *Student Member, IEEE*, Marjan Popov, *Fellow, IEEE*, and Aleksandra Lekić, *Senior Member, IEEE*

2024 IEEE PES Innovative Smart Grid Technologies Europe (ISGT EUROPE) | 978-1-7281-5207-3/24/$31.00 ©2024 EU | DOI: 10.1109/ISGTEUROPE62998.2024.10863193

***Abstract*—The stability of an HVDC transmission network is very important for the reliable transfer of power from renewable energy resources. Therefore, this paper proposes a region of attraction stability analysis method for grid-forming-based modular multilevel converters. The grid forming control uses a model predictive control-based controller for the inner current loop. The stability analysis is carried out using the direct Lyapunov method. For the model predictive control, the modified version of the cost function is used; the same function is also used as the cost function for the direct Lyapunov method. Furthermore, the boundaries formed by the limiters and Lyapunov function entirely explain transient event behavior.**

***Index Terms*—HVDC, MTDC, MMC, Grid Forming Control (GFM), Virtual Synchronous Machine, Lyapunov Stability, Large Signal Stability, Region of Attraction, RSCAD/RTDS®.**

I. Introduction

Stability analysis is crucial for ensuring the reliability of power system networks. Large-signal transient stability analysis has become more significant due to the increasing presence of converter-based generation [1]. The Direct Lyapunov function is a widely used metric for analyzing transient stability[2]. This metric can be further enhanced by applying the concept of the Region of Attraction. The presented analysis provides useful insight into the network behavior during large disturbances, making it an essential tool for power system stability analysis when dealing with Electro-Magnetic Transient (EMT) studies.

For a Modular Multi-level Converter (MMC)-based High Voltage Direct Current (HVDC) transmission network with grid forming control (GFM), voltage stability becomes very important as it focuses on maintaining an acceptable voltage during disturbances [3]. The existing literature on power system stability analysis has primarily focused on single Voltage Source Converter (VSC) stations connected to an infinite bus, where the injected power is ideal without harmonics [4]. However, the model used in this paper considers power injection from an aggregated model of an offshore wind farm, which includes harmonics and realistically represents the power injected into an HVDC transmission network. Additionally, this model involves a four-terminal network with a DC Hub, which is different from the point-to-point models that can be typically found in the literature. The control strategies employ Model Predictive Control (MPC)-based controllers, which are nonlinear controllers; the optimized nonlinear controllers reach new steady states faster when disturbed as compared to linear controllers like PI [5]. There is a need for further research on MPC-based controllers regarding large signal stability for transient events using the Direct Lyapunov method. Small signal stability analysis done with eigenvalue analysis typically focuses on a system's stable operating point. However, this method may not accurately predict system behavior under large disturbances[6]. Hence, a time-dependent analysis like transient large signal stability is necessary when dealing with transient events. This paper discusses the behavior of the network during transient events considering the variation of Short Circuit Ratios using the Region of Attraction plots. Furthermore, a sensitivity analysis is conducted on the outer loop control of the grid forming control strategy (i.e. Virtual Synchronous Machine (VSM)) and the controller parameters (MPC and PI). The study also considers the stability analysis of a GFM bipolar MMC with a metallic return, which is not commonly studied in the existing literature. Additionally, frequency-dependent phase cables are applied to consider the network's more realistic behavior. Overall, this research contributes to a better understanding the power system stability analysis under realistic and challenging scenarios. The Network is simulated in a real-time environment with the help of RSCAD/RTDS®.

The layout of this paper is as follows: Section II describes the Multi-Terminal high voltage Direct Current (MTDC) network/model and the mathematical model of an MMC. The GFM strategy used is discussed in Section III. The controllers implemented and compared, as well as PI and MPC, are presented in Section IV. The boundary formation using Region of attraction studies is presented and discussed in Section V, and Section VI discusses the stability analysis results. Finally, the paper ends with conclusions presented in Section VII.

II. Network Model

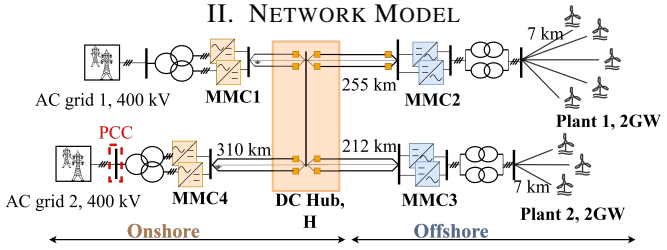

Fig. 1: A four-terminal ±525 kV bipolar half-bridge MMC-based HVDC system with a metallic return and a DC Hub. See Table I for specifications.

Fig. 1 shows the single-line network diagram, and Table I provides the network specification. The model of the MMC used in this network is shown in Fig. 2. Each MMC has three legs, and each leg consists of two arms. Each arm of the MMC has N_{SM} submodules (SM). The variables shown in Fig. 2 are defined for all three phases, i.e., $j \in \{a, b, c\}$. Half-bridge submodules (SMs) are represented by their averaged

R. Kamat Tarcar, A. Shetgaonkar, M. Popov, and A. Lekić are with the Faculty of Electrical Engineering, Mathematics and Computer Science, Delft University of Technology, Delft CD 2628, The Netherlands (e-mail: {R.KamatTarcar, A.D.Shetgaonkar, M.Popov, A.Lekic}@tudelft.nl).

979-8-3503-9042-1/24/$31.00©2024 European Union

TABLE I: Network specifications

Parameter	Onshore	Offshore
Transformer capacity	6 GW	4 GW
Rated grid line-line voltage	400 kV	66 kV
Transformer voltage ratio	400/275 kV	275/66 kV
Transformer leakage reactance	0.18 pu	0.15 pu
Transformer configuration	Yn/Δ, 1P3W	Δ/Yn, 3P2W
DC line inductances	80 mH	80 mH
No. of MMC Submodules	240	240
Submodule capacitance	25 mF	16 mF
Converter Inductance	50 mH	50 mH

equivalents, with R_{arm} and L_{arm} being the resistance and inductance, respectively. Each SM has capacitance C_{SM}. The converter model is developed according to [7]. By using the $\Sigma - \Delta$ nomenclature, the variables in the upper and lower converter arms can be represented as:

$$i_j^{\Delta} = i_j^U - i_j^L, \quad i_j^{\Sigma} = \frac{i_j^U + i_j^L}{2}, \tag{1}$$

$$v_{Mj}^{\Delta} = \frac{-v_{Mj}^U + v_{Mj}^L}{2}, \quad v_{Mj}^{\Sigma} = \frac{v_{Mj}^U + v_{Mj}^L}{2}. \tag{2}$$

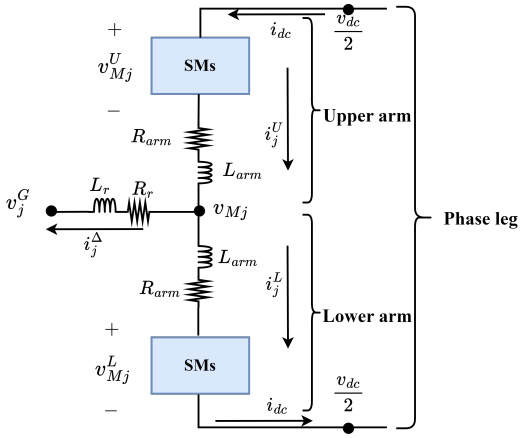

Fig. 2: Diagram of one MMC leg, for $j \in \{a, b, c\}$.

By applying the Clarke-Park Transforms (ABC to DQZ frame transformation) [7], the set of differential equations can be written in the d-q domain:

$$\frac{d}{dt}\left(\vec{i}_{dq}^{\Delta}\right) = \frac{\vec{v}_{Mdq}^{\Delta} - \left(\omega L_{eq}^{ac} J_2 + R_{eq}^{ac} I_2\right)\vec{i}_{dq}^{\Delta} - \vec{v}_{dq}^{G}}{L_{eq}^{ac}}, \tag{3}$$

$$\frac{d}{dt}\left(\vec{v}_{dq}^{\Delta}\right) = \omega J_2 \vec{v}_{qd}^{\Delta} + \frac{N_{SM}}{C_{SM}}\vec{i}_{dq}^{\Delta}, \tag{4}$$

where $L_{eq}^{ac} = L_r + \frac{L_{arm}}{2}$, $R_{eq}^{ac} = R_r + \frac{R_{arm}}{2}$, $J_2 = \begin{bmatrix} 0 & 1 \\ -1 & 0 \end{bmatrix}$, and I_2 is an identity matrix with the size 2×2.

III. Control Strategy

A GFM in the form of a Virtual Synchronous Machine (VSM) is used in this work and is depicted in Fig.3. VSM primarily produces the phase angle (θ) imperative for the dq transformation. This is realized by using the Swing equation of a synchronous machine, which is modified to include damping, expressed as:

$$2H\frac{d\omega_{VSM}}{dt} = P^*(t) - P(t) + K_d\left(\omega_{VSM} - \omega_{base}\right) \tag{5}$$

where H is the virtual inertia constant, set to $5s$. In (5), θ_{VSM} is the phase angle generated by the VSM. Furthermore, $\omega_{base} = 2\pi f$, where f is the grid's nominal frequency (50 Hz). K_d is the damping constant, which is set to 53 p.u. Fig. 3 is the block diagram of equation 5. For the GFM converter station to achieve the transfer of power from offshore MMC stations to the connected AC grid-connected, Fig.1, the standard VSM control strategy needs to be modified before it can be implemented. This is done so that the current injected into the grid can be limited, and the power factor of the MMC station can be improved. This modification, Fig. 4, is derived from [8], [9], which exhibits current limiting control. This modification involves using a virtual capacitor (C_v) to decouple the voltage control loop and implement a current limiting algorithm similar to that in a grid following a control strategy. Also, in Fig. 4, v_{rms}^* is the reference voltage signal which is set at 1 p.u., v_{rms} is the rms AC voltage which is to be controlled, $v_{d,q}^G$ are the AC voltages in dq domain, and v_d^{G*} is set to $zero$.

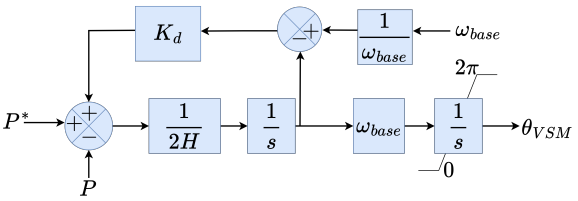

Fig. 3: Phase angle (θ) generation using VSM.

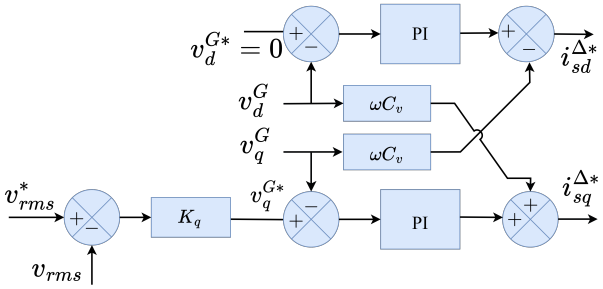

Fig. 4: The grid forming voltage control loop with a virtual capacitor.

IV. Controllers Implemented

A. Formulation of PI-based controller

Due to its simplicity and effectiveness, the PI-based controller is a widely accepted technique to regulate the performance of MMCs. These controllers are designed to maintain desired set-points for critical variables and to ensure stable and accurate network operation. The proportional term of the PI controller offers a control action corresponding to the error between the desired set-point and the actual value of the controlled signal. This provides a suitable response to system changes, which helps to reduce steady-state errors [10]. Meanwhile, the Integral term is responsible for the accumulated error over time, ensuring that any long-term steady-state errors are corrected by modifying the control action. Thereby eliminating residual offsets and enhancing the system's stability and accuracy. By tuning the proportional and integral gains of the controller, a reliable and robust control mechanism for MMC HVDC networks is provided.This enables precise regulation

of variables, effective rejection of disturbances, and improved system performance [11]. The physical definitions that govern the PI-based control loops are: $\Delta i_d^{\Delta ref} = \frac{1}{V_{dc}}(P^* - P)$,and $\Delta i_q^{\Delta ref} = \frac{\Delta V_{ac}}{\omega L_{eq}^{ac}}$.

B. Formulation of MPC

Model predictive control gains popularity and is widely used to control power converters [12]. A plant model forecasts the control inputs of model predictive control (MPC). This model acts as a mathematical replica, where the model outputs are used as inputs for the plant, and the plant outputs are then fed back as inputs to the model. In the MMC, MPC is implemented for the inner loop, to regulate the MMC's currents.

The continuous-time model equation must be transformed into a discrete-time state-space model to use MPC on MMC. This model is achieved by using the zero-order hold discretization method and augmented in the rate-based state space equations [13], where vector $\vec{x}(k) = \begin{bmatrix} i_d^\Delta & i_q^\Delta & i_{dB}^\Delta & i_{qB}^\Delta \end{bmatrix}^T$ represents state space variables and $\vec{u}(k) = \begin{bmatrix} v_{Md}^\Delta - v_d^G, v_{Mq}^\Delta - v_q^G, v_{MdB}^\Delta - v_{dB}^G, v_{MqB}^\Delta - v_{qB}^G \end{bmatrix}^T$ input variables, where the subscript B represents the negative or lower MMC in the bipolar configuration. State-space matrices are:

$$A = \begin{bmatrix} -\frac{R_{eq}^{ac}}{L_{eq}^{ac}} & -\omega & 0 & 0 \\ \omega & -\frac{R_{eq}^{ac}}{L_{eq}^{ac}} & 0 & 0 \\ 0 & 0 & -\frac{R_{eq}^{ac}}{L_{eq}^{ac}} & -\omega \\ 0 & 0 & \omega & -\frac{R_{eq}^{ac}}{L_{eq}^{ac}} \end{bmatrix} \tag{6}$$

$B = \operatorname{diag}\left\{\frac{1}{L_{eq}^{ac}}, \frac{1}{L_{eq}^{ac}}, \frac{1}{L_{eq}^{ac}}, \frac{1}{L_{eq}^{ac}}\right\}$, $C = A$ and $D = 0$. The MMC's AC side and DC side equations are discretized using the zero-order hold discretization method and augmented in the rate-based state space equations [13] using the solutions of the differential equations.

The MPC's cost function is formulated with a Linear Quadratic Regulator (LQR) as a base, subjected to equality and inequality constraints:

$$\min J = \sum_{i=1}^{N_p} ||\overrightarrow{x_m}(k+i \mid k)||_Q^2 + ||\Delta\vec{u}(k)||_R^2, \tag{7}$$

where $\overrightarrow{x_m}(k+i \mid k) = \overrightarrow{y_m^*}(k) - \overrightarrow{y_m}(k \mid k)$, and the expression definition is $||x||_U^2 = x^T U x$. Here, $Q \succeq 0$ and $R \succ 0$ are weighting matrices, and N_p is the prediction horizon. For the state variables $\overrightarrow{x_m}(k)$ the reference is $\overrightarrow{y_m^*}(k)$, and $\overrightarrow{y_m}(k)$ is the output variable of the plant.

The constraints for the control input are $\vec{i}_{dq}^{\Delta} \in [-\vec{1} \times 1.1$ p.u., $\vec{1} \times 1.1$ p.u.]. These constraints are the ones used in the PI-based controller to limit the $\vec{i}_{dq}^{\Delta}$ currents based on the IGBT current limits in the SMs of the MMCs, based on limitation standards for HVDC power systems.

V. Region of Attraction

The outer or secondary stability boundary is set by considering the impacts of the dq-current limiters and the threshold current values:

$$\vec{i}_{\mathrm{dq}}^{\Delta} = \min\left\{\vec{i}_{dq}^{\Delta ref}, \vec{i}_{dq}^{\Delta max}\right\}.$$

For the ROA estimation, the error in the signals is expressed by:

$$E = \begin{bmatrix} e_{1,2,3,4} \\ e_{5,6,7,8} \end{bmatrix} = \begin{bmatrix} i_x^\Delta - i_x^{\Delta *} \\ v_x^G - v_x^{G*} \end{bmatrix}, \quad f = \begin{bmatrix} f_{1,2} \\ f_{3,4} \end{bmatrix} = \begin{bmatrix} e_{6,5} \\ e_{8,7} \end{bmatrix}, \tag{8}$$

where $x \in \{d, q, dB, qB\}$. After substituting the error terms in equations (3)-(4), we obtain:

$$\frac{de_i}{dt} = \frac{\vec{v}_{dq}^{\Delta M} - \left(\omega L_{eq}^{ac} J_2 + R_{eq}^{ac} I_2\right) e_i - e_{i+4}}{L_{eq}^{ac}}, \tag{9}$$

$$\frac{d}{dt}\left(e_{i+4}\right) = \omega J_2 f_i + \frac{N_{SM}}{C_{SM}} e_i, \tag{10}$$

where the subscript $i \in \{1, 2, 3, 4\}$.

The energy function selected for this analysis is the MPC's cost function, which can be reformulated as $W(e) = E^T M E \geq 0$, where $M \succ 0$ is the positive definite matrix defined as $M = \frac{1}{2}\operatorname{diag}\left\{L_{eq}^{ac}, L_{eq}^{ac}, L_{eq}^{ac}, L_{eq}^{ac}, C_{SM}, C_{SM}, C_{SM}, C_{SM}\right\}$. In this way, the quadratic Lyapunov energy function is obtained as [14] for the HVDC system under study, which is expressed as:

$$W(\tilde{e}) = \frac{1}{2}\sum_{j=1}^{4} L_{eq}^{ac} e_j^2 + \frac{1}{2}\sum_{j=5}^{8} C_{SM} e_j^2. \tag{11}$$

The derivative of the equation is: $\frac{dW(\tilde{e})}{dt} = \sum_{j=1}^{4} L_{eq}^{ac} e_j \frac{de_j}{dt} + \sum_{j=5}^{8} C_{SM} e_j \frac{de_j}{dt}$, and it has to be negative in the case of a stable system. To eliminate the derivative terms on the right-hand side, equations (9) and (10) are substituted to obtain:

$$\begin{aligned} \frac{dW(\tilde{e})}{dt} &= -\sum_{j=1}^{4} R_{eq}^{ac} e_j^2 + \sum_{j=5}^{8} \left(-e_j + N e_j\right) e_{j-4} \\ &\quad + \left(v_d^M e_1 + v_q^M e_2 + v_{dB}^M e_3 + v_{qB}^M e_4\right), \end{aligned} \tag{12}$$

$$-R_{eq}^{ac} e_i^2 < 0, \qquad \left((N-1)e_{i+4} + v_z^M\right) e_i = \alpha_i e_i^2, \tag{13}$$

for $i \in \{1, 2, 3, 4\}$ and $z \in \{d, q, dB, qB\}$. The values of α_i are selected based on the applied control strategy, such that the derivative of the Lyapunov function is negative, creating a boundary in the shape of a circle with a radius of 0.3. The resulting Lyapunov function is semi-definite within the circle's boundaries for these conditions, as seen in Fig. 5. The region between the circle and the boundary formed by the limiters causes sustained oscillations, causing the system to be in a limit cycle [15].

VI. Stability Analysis

The ROA stability analysis is carried out for the grid-forming MPC-based, PI-based MMCs and an unstable operation during a transient event in the form of a three-phase AC fault at the Point of Common Coupling (PCC), as shown in Fig.1. This event is studied for different values of SCRs, namely, $10, 5, 3, 2$ and 1.5.

Fig. 6 shows the AC voltage behavior and ROA assessment for a GFM with an MPC-based controller for various SCRs. Furthermore, Fig. 6b, shows the trajectory of the e_1 and e_2 with the corresponding ROA boundary during the transient event (which occurs in the interval between t_1 and t_2) highlighted in Fig. 7a. In Fig. 6b, $SEP1$ and $SEP2$ are the

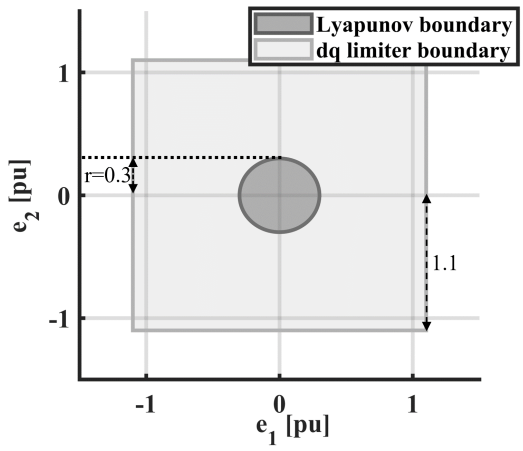

Fig. 5: Boundary of attraction depiction.

initial and final stable equilibrium points before and after the transient. $SEP1$ is the origin as the errors computed by (8) are $zero$ during steady state operation. It can be observed from varying the SCR in Figs. 6a and 6b that the trajectories of e_1 and e_2 seem to deviate from their initial $SEP1$ and move towards the edge of the Lyapunov boundary; as the SCR is decreased.

Fig. 7 shows the plot for a grid-forming converter with a PI-based controller. Furthermore, Fig. 7a shows the AC voltage behavior during the transient event for different SCRs; Fig. 7b illustrates the trajectory of the e_1 and e_2 during the transient event in three-dimensional phase plot with the ROA limits. In Fig. 7b, $SEP1$, and $SEP2$ are the initial and final stable equilibrium points plotted for time intervals t_1 and t_2 which showcase the transient event.$SEP1$ is the origin, so the errors computed in equation (8) are $zero$. An important observation is that the closer the point approaches the circle's (in this 3-dimensional figure, a cylinder) boundary, the damping capabilities of the control strategy are hampered, and more oscillations are observed, as shown in Fig. 7. The reason being that the Pi-based inner loop is not fast and robust enough to accommodate the rapid changes at low SCRs than an MPC-based inner loop.

Fig. 8 shows the AC voltage behavior and the ROA plots for an unstable case. The unstable case was simulated by reducing the H and K_d terms of the VSM equation, equation5. It shows that for lower SCRs, the limit cycle phenomenon becomes more visible as the oscillations become more prominent and the trajectories formed by e_1 and e_2 go beyond the Lyapunov boundary for the majority part of its course this can be seen in Fig. 8b. This can also be seen in the AC voltage waveform in Fig. 8. This solidifies the earlier observation that the damping weakens as it approaches the Lyapunov boundary. It is also observed that for $SCR = 1.5$ in Fig. 8b, the system becomes momentarily unstable as the trajectory goes beyond the boundary of the dq limiters. In this case, there is an Unstable Point ($UP1$), as the endpoint is beyond the Lyapunov boundary.

VII. Conclusion

This paper proposes a comprehensive ROA stability analysis based on the Lyapunov theory for MPC-based GFM MMCs. This is achieved based on the boundaries formed by the modified form of the MPC cost function used as an energy function. This function describes the detailed behavior of the system during transient events by linking the damping ability of the VSM GFM to the trajectories of the states defined in the error matrix (E) in the form of initial and final stable/unstable Equilibrium Points. It also acts as an indicator of post-transient state of stability or instability, based on the trajectories of the error matrix attributes, e_1 and e_2. The real-time simulations conducted on RSCAD/RTDS® validate the effectiveness of the boundaries established by the direct Lyapunov method and the Region of attraction consequently.

References

[1] C. Collados-Rodriguez, M. Cheah-Mane, F. Cifuentes-Garcia, E. Prieto-Araujo, O. Gomis-Bellmunt, L. Coronado, C. Longás, S. Sanz, M. Martín, and A. Cordón, "Integration of an MMC-HVDC link to the existing LCC-HVDC link in Balearic islands based on Grid-following and Grid-forming operation," *IEEE Transactions on Power Delivery*, vol. 37, no. 6, pp. 5278–5288, 2022.

[2] C. Andic, A. Ozturk, and B. Turkay, "Rotor Angle Stability Analysis by using Lyapunov's Direct Method of a SMIB power system," in *2022 4th Global Power, Energy and Communication Conference (GPECOM)*, 2022, pp. 296–300.

[3] H. Cheng, Z. Shuai, C. Shen, X. Liu, Z. Li, and Z. J. Shen, "Transient Angle Stability of paralleled Synchronous and Virtual Synchronous Generators in islanded Microgrids," *IEEE Transactions on Power Electronics*, vol. 35, no. 8, pp. 8751–8765, 2020.

[4] Y. Wang, H. Sun, S. Xu, and B. Zhao, "Transient Stability Analysis and Improvement for the Grid-Connected VSC system with Multi-Limiters," *IEEE Transactions on Power Systems*, vol. 39, no. 1, pp. 1979–1995, 2024.

[5] A. Pavlov, B. Hunnekens, N. Wouw, and H. Nijmeijer, "Steady-state performance optimization for nonlinear control systems of lur'e type," *Automatica*, vol. 49, no. 7, pp. 2087–2097, 2013. [Online]. Available: https://www.sciencedirect.com/science/article/pii/S000510981300229X

[6] H. Wang, H. Sun, and X. Lu, "An Overview on Small-Signal Modeling and Stability Analysis Methods of Voltage-Source Converter Grid-Connected System," in *2021 3rd Asia Energy and Electrical Engineering Symposium (AEEES)*, 2021, pp. 320–326.

[7] G. Bergna-Diaz, J. Freytes, X. Guillaud, S. D'Arco, and J. A. Suul, "Generalized voltage-based state-space modeling of modular multilevel converters with constant equilibrium in steady state," *IEEE Journal of Emerging and Selected Topics in Power Electronics*, vol. 6, no. 2, pp. 707–725, 2018.

[8] J. Freytes, J. Li, G. D. Preville, and M. Thouvenin, "Grid-Forming Control with Current Limitation for MMC under Unbalanced Fault Ride-Through," *IEEE Transactions on Power Delivery*, vol. 36, pp. 1914–1916, 6 2021.

[9] T. Qoria, E. Rokrok, A. Bruyere, B. Francois, X. Guillaud, S. Member, B. François, and S. Member, "Grid-Forming Control with Decoupled Functionalities for High-Power Transmission System Applications," *IEEE Access*, vol. 8, pp. 197 363–197 378, 2020. [Online]. Available: https://hal.archives-ouvertes.fr/hal-03703440

[10] C. Kadu and C. Patil, "Design and Implementation of stable PID controller for Interacting level Control System," *Procedia Computer Science*, vol. 79, pp. 737–746, 2016, proceedings of International Conference on Communication, Computing and Virtualization (ICCCV) 2016.

[11] S. Thomsen, N. Hoffmann, and F. W. Fuchs, "PI control, PI-based State Space Control, and Model-Based Predictive Control for Drive Systems with Elastically Coupled Loads—a comparative study," *IEEE Transactions on Industrial Electronics*, vol. 58, no. 8, pp. 3647–3657, 2011.

[12] S. Du, A. Dekka, B. Wu, and N. Zargari, *Modular multilevel converters: analysis, control, and applications*. John Wiley & Sons, 2018.

[13] A. Shetgaonkar, L. Liu, A. Lekić, M. Popov, and P. Palensky, "Model predictive control and protection of MMC-based MTDC power systems," *International Journal of Electrical Power & Energy Systems*, vol. 146, p. 108710, 2023.

[14] R. Janbazi Ghadi, M. Mehrasa, M. Ebrahim Adabi, and S. Bacha, "Lyapunov theory-based control strategy for multi-terminal MMC-HVDC systems," *International Journal of Electrical Power & Energy Systems*, vol. 129, p. 106778.

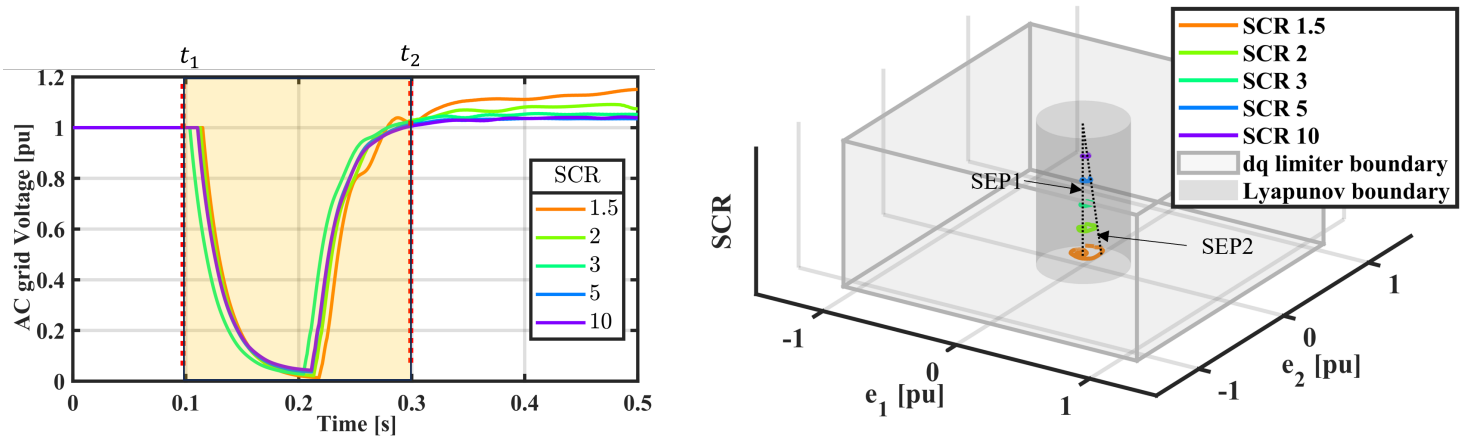

(a) Three Phase fault

(b) Region of Attraction plot for MPC

Fig. 6: MMC with grid forming control strategy and MPC controller

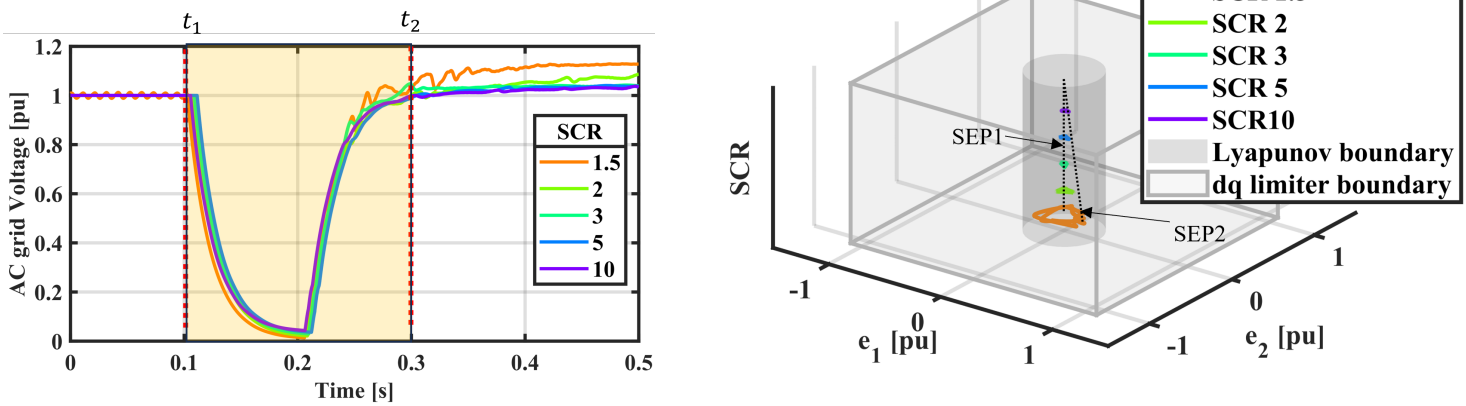

(a) Three Phase fault

(b) Region of Attraction plot for PI

Fig. 7: MMC with grid forming control strategy and PI controller.

[15] C. W. d. Silva, "Sensors for control," in *Encyclopedia of Physical Science and Technology (Third Edition)*, third edition ed., R. A. Meyers, Ed. Academic Press, pp. 609–650. [Online]. Available: https://www.sciencedirect.com/science/article/pii/B0122274105001393

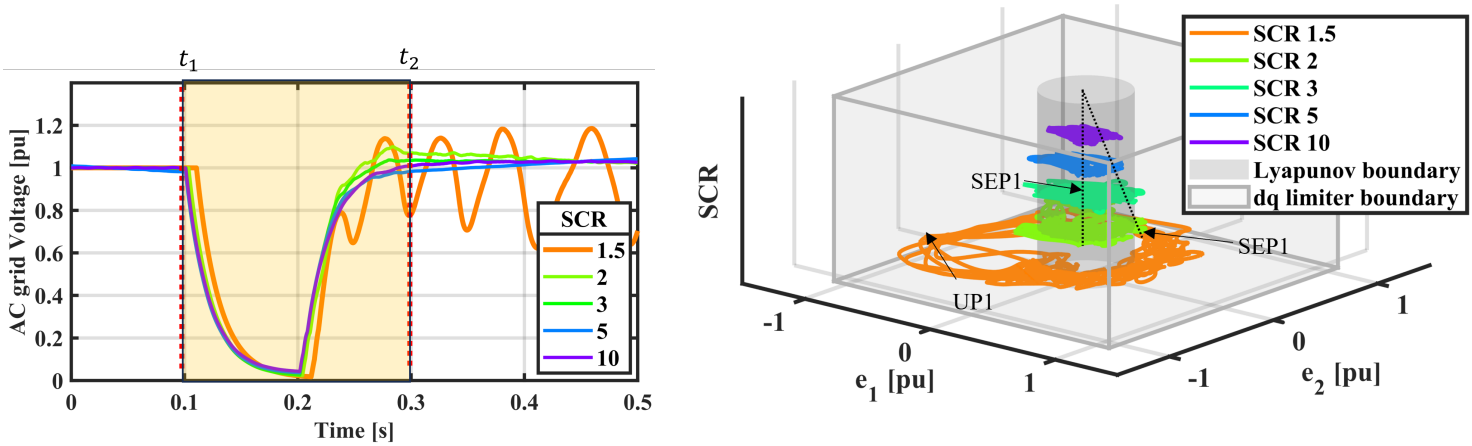

(a) Three Phase fault

(b) Region of Attraction plot for the unstable case

Fig. 8: MMC with grid forming control strategy for the unstable case.